Toxicity of silver nanoparticles in human macrophages: uptake, intracellular distribution and cellular responses

2011 J. Phys.: Conf. Ser. 304 012030

(http://iopscience.iop.org/1742-6596/304/1/012030)

Journal of Physics: Conference Series **304** (2011) 012030 doi:10.1088/1742-6596/304/1/012030

Toxicity of silver nanoparticles in human macrophages: uptake, intracellular distribution and cellular responses

A Haase[1], J Tentschert[1], H Jungnickel[1], P Graf[2], A Mantion[3], F Draude[4], J Plendl[5], M E Goetz[1], S Galla[4], A Mašić[6,7], A F Thuenemann[3], A Taubert[6,7], H F Arlinghaus[4] and A Luch[1]

[1]BfR — Federal Institute for Risk Assessment, Department of Product Safety, Thielallee 88-92, 14195 Berlin, Germany

[2]University of Basel, Department of Chemistry, Klingelbergstrasse 80, 4056 Basel, Switzerland

[3]BAM — Federal Institute for Materials Research and Testing, Richard-Willstätter-Strasse 11, 12489 Berlin, Germany

[4]University of Münster, Institute of Physics, Wilhelm Klemm Strasse 10, 48149 Münster, Germany

[5]Free University of Berlin, Department of Veterinary Medicine, Institute of Veterinary Anatomy, Koserstrasse 20, 14195 Berlin, Germany

[6]University of Potsdam, Institute of Chemistry, Karl- Liebknecht- Strasse 24-25, 14476 Potsdam-Golm, Germany

[7]Max-Planck-Institute of Colloids and Interfaces, Am Mühlenberg 2, 14476 Potsdam-Golm, Germany

E-mail: andrea.haase@bfr.bund.de; alexandre.mantion@bam.de

Abstract. Silver nanoparticles (SNP) are among the most commercialized nanoparticles worldwide. They can be found in many diverse products, mostly because of their antibacterial properties. Despite its widespread use only little data on possible adverse health effects exist. It is difficult to compare biological data from different studies due to the great variety in sizes, coatings or shapes of the particles. Here, we applied a novel synthesis approach to obtain SNP, which are covalently stabilized by a small peptide. This enables a tight control of both size and shape. We applied these SNP in two different sizes of 20 or 40 nm (Ag20Pep and Ag40Pep) and analyzed responses of THP-1-derived human macrophages. Similar gold nanoparticles with the same coating (Au20Pep) were used for comparison and found to be non-toxic. We assessed the cytotoxicity of particles and confirmed their cellular uptake via transmission electron microscopy and confocal Raman microscopy. Importantly a majority of the SNP could be detected as individual particles spread throughout the cells. Furthermore we studied several types of oxidative stress related responses such as induction of heme oxygenase I or formation of protein carbonyls. In summary, our data demonstrate that even low doses of SNP exerted adverse effects in human macrophages.

1. Introduction

Due to their unique optical, catalytical and disinfectant properties silver nanoparticles (SNP) gain high commercial and scientific interest. They are used for many different applications and in a wide range of different products [1,2] ranging from wound dressing, coatings of surgical instruments and prostheses [3,4] to the use in food container systems or as coating material for certain household devices such as washing machines. They are incorporated into textiles [5,6] and also added to cosmetics [7]. Besides that they are highly attractive for creation of novel and advanced functional materials.

Serious concerns about putative toxicological and environmental effects have been raised [8-10]. Recently different reports demonstrate that incorporation of SNP into organisms is possible via different routes and systemic dissemination can occur. Thus SNP are likely to reach secondary target organs. In an inhalation study in rats SNP could be detected in lung tissue, but also in liver and brain [11]. After subcutaneous injection SNP were found in kidney, liver, spleen, lung and brain [12]. In contrast to nanoscaled titanium dioxide dermal uptake has been proven for SNP [13]. Although acute toxic effects could not be detected *in vivo*, systemic distribution and accumulation in certain tissues could lead to chronic toxicity. Different *in vitro* studies could clearly demonstrate adverse effects of SNP in various types of cells including human mesenchymal stem cells [14], THP-1-derived macrophages [15], human lung fibroblasts and glioblastoma cells [16] as well as alveolar macrophages [17]. The development of oxidative stress and in particular the generation of reactive oxygen species (ROS) represents the model mostly used to explain the *in vitro* toxicity of nanoparticles[18]. Generation of ROS is also assumed to be underlying the toxicity of SNP [17,19]. This could occur via different mechanisms. First, nanoparticles could catalyze redox reactions directly on their surface leading to ROS formation. Another mechanism that might be of particular relevance for silver is based on direct interactions with mitochondrial membrane proteins, which often contain sulfur-containing amino acids. Disturbance of mitochondrial functions can lead to increased production of ROS.

SNP belong to the group of nanoparticles with moderate solubility. As consequence, silver ions are being released and thus could also contribute to toxic reactions in cells [20]. It is still an ongoing discussion whether toxicity is caused by particles as such, or by silver ion release from silver nanoparticles, or both [21]. Usually nanotoxicity studies remain to suffer from several discrepancies and irreproducibilities. SNP can be produced via different synthesis routes in a great variety of forms with different coatings, shapes and sizes. Often characterization data of those particular nanoparticles applied in a specific study are incomplete. However it is well known that each of these particle properties strongly affects the biological responses, as has been already shown for size-dependent reactivity [17,22], coating- or surface-dependent reactivity [23], or shape-dependent properties [24] of SNP. With classical synthesis approaches, such as citrate reduction, the properties of the resultant particles cannot be sufficiently controlled or modified. This usually results in preparations with broad variance in nanoparticle sizes and large polydispersity indices. Significant batch-to-batch variations are often detected as well. Thus the relationship between particle properties and toxicological responses usually remains ambiguous and structure-reactivity correlations cannot be trustfully demonstrated. In nanotoxicology it thus becomes crucial to tightly control and direct syntheses routes of particles toward desired well-defined properties and to fully characterize the resulting particles regarding their physicochemical properties prior to its application in biological systems. Recently the application of peptides as structure-directing agents gained highest interest. Certain peptides can be used to control the growth of inorganic materials [25,26] or of complex silver-peptide hybrids [27]. Here we used a novel type of SNP, which are made of a silver nanoparticle core surrounded by a small peptidic shell [28]. These particles display a narrow size distribution and possess a defined shape. The particles can be easily obtained in a reproducible way and in large quantities. In aqueous preparations they constitute stable and monodispersed suspensions, thus making them highly suitable for toxicological testing in cell culture systems. In the present study we use peptide-coated SNP in toxicity

assays *in vitro* and compare the outcome with effects of corresponding gold nanoparticles of same size and coating.

2. Materials and methods

2.1. Nanoparticle preparation

Chemicals were purchased from Fluka (Buchs, Switzerland) or Bachem (Bubendorf, Switzerland) and used without further purification. All amino acids were L-isomers. The peptide sequence is shown in Figure 1. Nanoparticles were prepared according to an in-house protocol, and characterized as published [28]. The nanoparticles became available in two sizes, *i.e.*, 20 nm (Ag20Pep) and 40 nm (Ag40Pep), respectively. The peptide-coated gold nanoparticles (Au20Pep) were prepared by ligand exchange of 20 nm citrate-coated gold nanoparticles with the peptide CKK.

2.2. Cell culture

The THP-1 cell line was obtained from the German Collection of Microorganisms and Cell Cultures GmbH (DSMZ, Braunschweig, Germany). Cells were grown at 37°C with 5% CO_2 in RPMI medium supplemented with 10% fetal calf serum, 2 mM L-glutamine, 10 mM HEPES, 1 mM pyruvate, 100 U/ml penicillin and 0.1 mg/ml streptomycin. Differentiation into macrophage-like cells was performed by adding 100 ng/ml phorbol-12-myristate-13 acetate as described in the literature [35,36].

2.3. Cytotoxicity tests

Cell vitality after nanoparticle treatment was determined using WST-1 assay (Roche Applied Biosystems) according to the manufacturer's instructions with modifications to adapt for nanoparticle-treated cells. Briefly, cells were seeded in a 96-well plate with a density of 1 x 10^4 cells per well, differentiated and incubated with nanoparticles (4 replicates per concentration). After 24 or 48 h, WST-1 reagent was added to the cells, and after color reaction the resulting solution was centrifuged to remove the physically interfering nanoparticles. Finally spectrophotometric evaluation was performed. The relative viability (% viability compared to untreated cells) was calculated as mean value ± standard error of the mean (SEM) as a result of at least 3 independent experiments. The LDH assay was performed using a standard LDH assay from Promega (Mannheim, Germany) according to the manufacturer's instructions. The results shown represent mean values ± SEM of at least 3 independent experiments.

2.4. Transmission electron microscopy

TEM analysis was performed as previously described [37]. Cells in the culture dish were washed with phosphate buffered saline (PBS) and fixed by immersion with Karnovsky's fixative at 4°C. After three washing steps in 0.1 M cacodylate buffer, postfixation was performed with 2% osmium tetroxide in 0.1 M cacodylate buffer for 1 h at 4°C. After another three washing cycles in 0.1 M cacodylate buffer, cells were removed from the culture dish and centrifuged at 2000 x *g* for 5 min. The pellet was then coated with 1.5% agar (Merck Eurolab, Darmstadt, Germany) for 30 min at 4°C. Subsequently the agar with the attached cell layer was removed from the wells. The samples were dehydrated in an ascending ethanol series (30-100% alcohol v/v) and embedded in Epon using beem capsules (Plano, Marburg, Germany). Polymerization was carried out at 60°C for 24 h. Semithin sections (1 µm) were cut on an Ultracut E ultramicrotome (Reichert-Jung, Vienna, Austria) with a diamond knife, stained as published elsewhere [34] and analyzed by light microscopy. Ultrathin sections (60 nm) were cut with a diamond knife, mounted on copper grids (Plano, Marburg, Germany) and examined with a Zeiss 10CR electron microscope (Jena, Germany).

2.5. Confocal Raman microscopy

After fixation with 4% paraformaldehyde cells were investigated with a confocal Raman microscope (CRM300, WITec, Ulm, Germany) equipped with a piezo-scanner (P-500, Physik Instrumente,

Karlsruhe, Germany), a 60x objective, and a 532 nm Nd:YAG laser. Spectra were acquired with an air-cooled CCD detector (DU401-BV, Andor, UK) with 600 gratings/mm (UHTS 300, WITec, Germany). ScanCtrlSpectroscopyPlus (version 2.04, WITec) was used for data acquisition and processing. Power was adjusted to provide a good signal-to-noise ratio and to avoid sample destruction. Typically, less than 1 mW full beam power was applied at the sample.

2.6. Cell lysates, SDS-PAGE, immunoblot and detection of protein carbonyls

Cells were washed with PBS three times and lysed by adding a modified RIPA buffer (50 mM Tris/HCl pH 7.4; 150 mM NaCl, 1 mM EDTA, 1% Igepal, 0.25% Na-deoxycholate). Lysates were centrifuged and stored at –80°C. Protein concentrations were determined through Bradford assay (BioRad, München, Germany) and SDS-PAGE was performed according to standard protocols. SDS-PAGE gels were transferred onto nitrocellulose membranes with a semidry blotting system. For 2D gel electrophoresis we used the system consisting of an IPGPHOR 3 unit and an EttanDALTtwelf of GE Healthcare (Freiburg, Germany). Proteins were precipitated and recovered in 2D lysis buffer containing 7 M urea, 2 M thiourea and 4% chaps. For the first dimension we used 24 cm IPG strips (pH 3-10, NL) and further steps were according to manufacturer's instructions. The gels were blotted with a semi-dry system as well. For detection of protein carbonyls OxyBlot Kit (Millipore, Schwalbach, Germany) was used. Antibodies against HO-1, tubulin or actin were obtained from Abcam (Abcam, Cambridge, UK). Images were obtained with a GelDoc system (BioRad, München, Germany) and analyzed with QuantityOne software.

2.7. Analysis of the protein corona of nanoparticles

Ag20Pep nanoparticles were incubated with complete cell culture medium containing 10% serum in a final concentration of 125 µg/ml for 2h. The particles were pelleted with table top centrifugation at 13.000 rpm for 15 min, washed once with PBS and eluted with Laemmli Buffer at 95°C for 5 min. The eluted proteins were separated via SDS-PAGE and stained with Coomassie dye. Images were captured with a BioRad GelDoc system and further analyzed with Quantity One Software (BioRad).

3. Results

3.1. Characterization of nanoparticles

Here we used the structure-directing activity of the central cystine residue as part of a dimer of the tripeptide CKK, along with ascorbate as reducing agent, to form SNP of well-defined sizes, shapes and coatings. The resultant nanoparticles and the structure of the peptide are explained schematically in Figure 1. Representative TEM pictures are shown in Figure 2. A single nanoparticle is composed of a silver metal core and a covalently attached peptidic layer made of the peptide CKK. X-ray photoelectron spectroscopy (XPS) revealed that this peptide becomes covalently linked to the metal surface through the *in situ* cleaved cystine bridge. Moreover, surface-enhanced Raman spectroscopy showed that the peptide is attached in a brush-like orientation, rather than enwrapping the metal core in a concentric manner. Thus, the silver nanoparticle is coated with a dense vertical layer of peptide molecules and only marginally covered at the surface by ascorbate. This indicates that the surface of the particles is tightly covered by a dense and covalently bound peptide, thus making a simple disintegration into silver ions unlikely.

Small-angle X-ray scattering (SAXS) and dynamic light scattering (DLS) were applied to characterize the colloidal properties of the nanoparticles in aqueous suspensions (Figure 3). SAXS demonstrated that the particle suspension is mainly monodisperse. The polydispersity index is only about 18% as it can be deduced from the minimum in the scattering curve. All nanoparticles synthesized have a narrow size range. Interestingly, the reason for this moderate polydispersity can be directly connected to the structural information obtained from Rietveld refinement of the powder diffraction pattern. The single crystallites are of an average size of 5 nm. This relates to both a

controlled size (dependent on the reaction conditions) and a controlled polydispersity, as the crystallite size is “pre-programmed” by the structure-directing properties of the peptide.

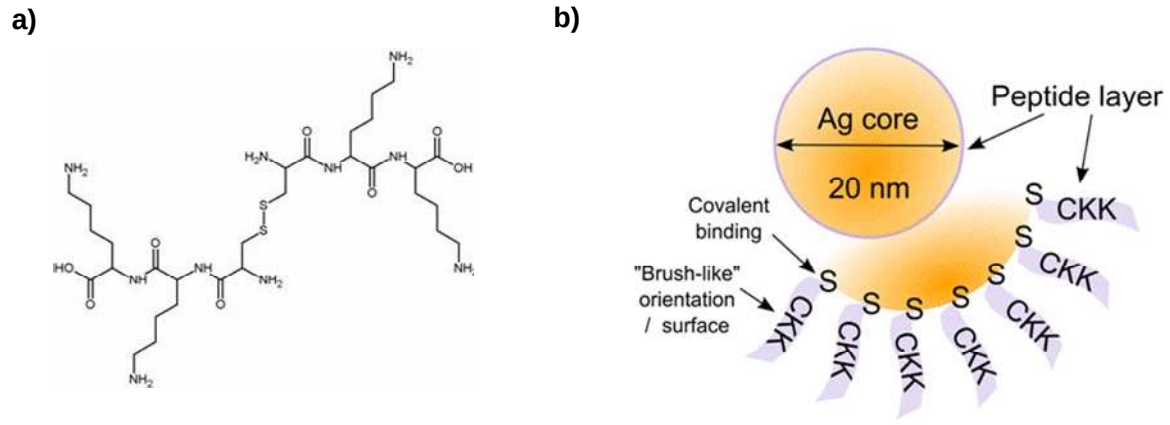

Figure 1. Structure of the peptide used for coating (a) and a scheme of the resultant nanoparticle (b).

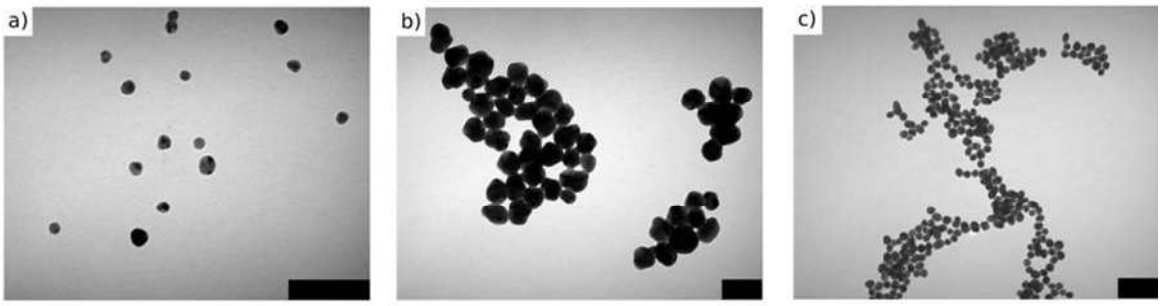

Figure 2. Representative TEM images of the particles produced: (a) Ag20Pep, (b) Ag40Pep, and (c) Au20Pep. The scale bar equals 100 nm in all images shown.

Both SAXS and DLS indicate a very similar size distribution of these particles (Figure 3, inset). DLS data in particular reveal that there are no larger aggregates present in solution. Interestingly, DLS also points to the presence of loose but concentration-dependent interactions between the nanoparticles, as could be inferred from the low q region in the SAXS curve. SAXS provides information about the electron-dense core as the organic shell is transparent to X-rays, while DLS provides information about the hydrodynamic radius of the nanoparticles. For round-shaped nanoparticles, the difference between both radii is directly related to the thickness of the shell. However, DLS results are influenced by (repulsive or attractive) interactions between the particles. Both techniques clearly show that the nanoparticles can be dispersed as single entities and that they do not coalesce to larger objects once being in solution.

Furthermore the covalently linked peptide helps to ensure several properties such as stability in the dry state, and the prevention of Ostwald ripening and ligand exchange at the surface. Importantly the interface is not passivated for further interactions with living organisms, as would be a polyethylene glycol layer repellant to proteins [29]. Furthermore the peptide could be used as a bio-interface to specifically target these nanoparticles or it can be useful for detection and purification of the particles.

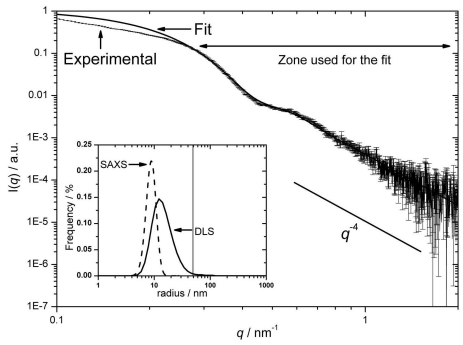

Figure 3. Small-angle X-ray scattering (SAXS) curve of Ag20Pep. Results of the fit are: 9.4 ± 0.2 nm and a polydispersity of σ = 18% using a Schultz sphere population model. Inset: size distribution as inferred from the SAXS curve and hydrodynamic radii as inferred from the DLS data, both volume-averaged. The straight line shows the limit upon which an object cannot be seen anymore at our SAXS settings.

3.2. Cytotoxicity of silver nanoparticles

We used macrophages derived from the human monocytic leukemia cell line THP-1 as a cellular model for toxicity testing. Since macrophages usually contribute to a first-line defence *in vivo* operating against foreign intruders such as systemically distributed nanoparticles they are of high relevance as model system. In addition they trigger subsequent immunological processes via secretion of cytokines. First we analyzed the nanoparticle-mediated cytotoxicity with a WST-1 viability assay. Cells were exposed for 24 or 48 h with increasing concentrations of silver or gold nanoparticles (Figure 4). Both types of SNP displayed strong cytotoxicity, which was dependent on dose and time of treatment. The smaller SNP (Ag20Pep) were slightly more toxic when compared to the larger counterparts (Ag40Pep) with respect to mass doses. The resultant IC(50) values after 24 h of exposure were 110 µg/ml (Ag20Pep) and 140 µg/ml (Ag40Pep), respectively. After 48 h of exposure the IC(50) values strongly decreased and were determined at 18 µg/ml (Ag20Pep) and 30 µg/ml (Ag40Pep), respectively. However, if the doses were calculated based on particle surface the viability curves and IC(50) values were in a similar range for both sizes of SNP (Figure 5). By contrast, gold nanoparticles proved mainly inert. Only at the highest concentrations tested little cytotoxicity could be observed, but viability was always higher than 80% (Figure 4).

In parallel we performed another, independent assay to measure cytotoxicity via quantifying the release of lactate dehydrogenase (LDH) into the supernatant (data not shown). Both assays provided comparable information. In addition we were interested in the mechanism of cell death. Therefore we measured the percentage of apoptotic cells after treatment with the different nanoparticles through propidium iodide/annexin V staining. Since apoptotic cells were virtually absent irrespective of the treatment conditions applied, we conclude that SNP-mediated cell death occurs via non-apoptotic pathways (data not shown).

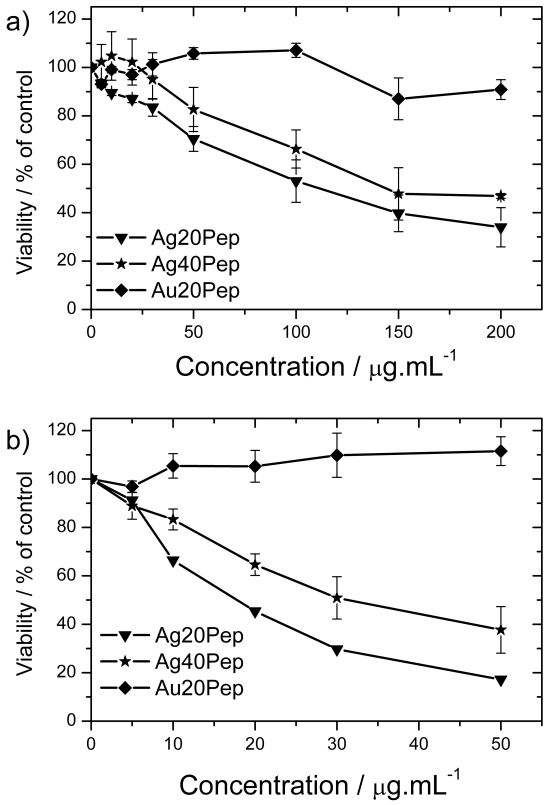

Figure 4. Measurement of viability after treatment of THP-1-derived macrophages with Ag20Pep, Ag40Pep or Au20Pep particles for 24 h (a) or 48 h (b).

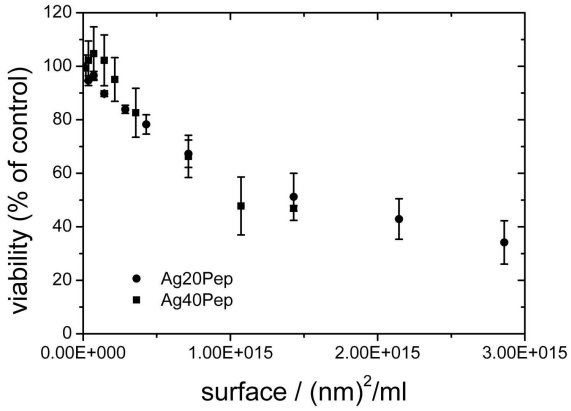

Figure 5. Calculation of cell viability after treatment with Ag20Pep or Ag40Pep particles. Data are derived from Figure 4 (WST-1 assay, 24 h exposure) and doses were calculated based on nanoparticle's surface and the assumption that particles are spherically shaped.

3.3. Visualization of particle uptake

We used transmission electron microscopy (TEM) to study nanoparticle-treated macrophages on an ultrastructural level (Figure 6). With TEM we could demonstrate that both sizes of SNP (20 nm and 40 nm) are efficiently taken up into macrophages. Virtually each cell analyzed was packed with SNP. We could detect some larger aggregates of SNP in the cytoplasm. However, the majority of SNP appeared as small and individual particles freely distributed throughout the cytoplasm, and without being surrounded by membrane envelopes. Furthermore SNP were detected in nuclei and even deep in the nucleoli, and inside lysosomes. Other organelles such as mitochondria or the endoplasmic reticulum were free of nanoparticles. Directly underneath the cellular membrane SNP were found

highly concentrated as individual particles, indicating that these particles have been freshly taken-up through a non-phagocytic mechanism.

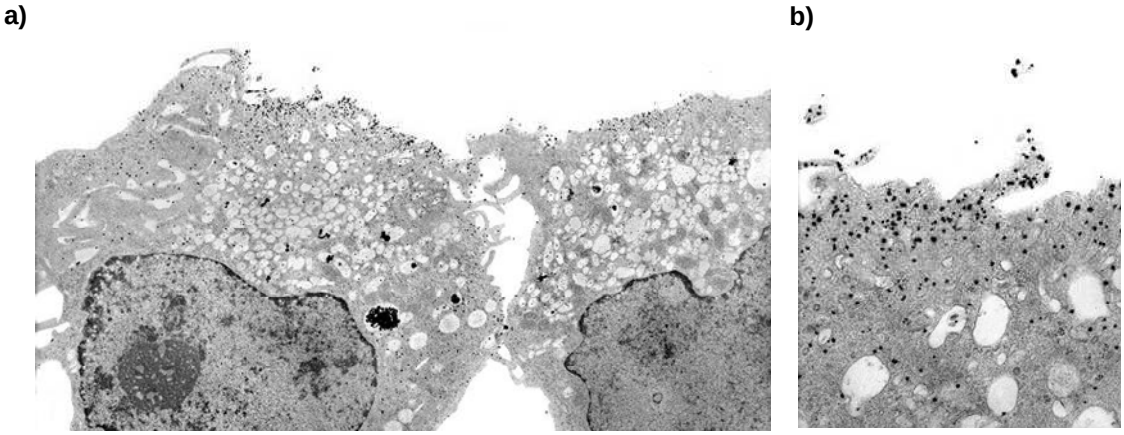

Figure 6. Transmission electron microscopy (TEM) images of macrophages upon exposure to Ag40Pep particles. (a) Overview of a treated cell (2.500x).
(b) Detailed picture of particles directly underneath the cell membrane (20.000x).
In each experiment cells were treated with 20 µg/ml SNP for 20 h.

Based on these findings we suggest that macrophages may ingest SNP through at least two different pathways. Aggregated SNP are possibly incorporated via phagocytosis while single nanoparticles might enter cells rather via non-phagocytic routes. Membrane flip-flop mechanisms or direct penetration via ion-channels are possible routes for passive and non-phagocytic uptake of SNP, but active transport routes might exist as well. Further experiments are needed to analyze these different possibilities.

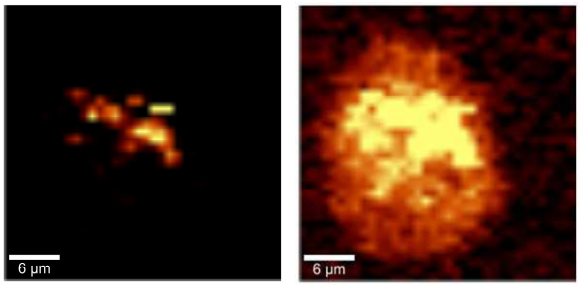

Figure 7. Confocal Raman image of a macrophage cell treated with 20 µg/ml Ag20Pep for 20 h. On the left side only signals from the nanoparticles are shown. The right side shows an overlay of signals originating from both nanoparticles and organic material inside the cell.

In addition, nanoparticles inside macrophages were visualized with confocal Raman microscopy (Figure 7). Due to the covalently linked peptide to the metal core the SNP prepared offered the advantage of being specifically detectable via induced metal-sulphur stretching vibrations monitored through confocal Raman microscopy.

Confocal Raman microscopy can be applied very fast without tedious sample preparation. Again, we detected a few number of large aggregates together with many smaller aggregates and countless individual SNP, the latter being spread throughout the entire cell.

3.4. Analysis of oxidative stress responses

Since exposure of cells to metal nanoparticles most likely results in the generation of oxidative stress we used different biochemical approaches to analyze this in more detail (Figure 8). Oxidative stress results from of an imbalance between the generation and elimination of reactive oxygen species (ROS)

within cells. Once generated ROS may then react fastly with cellular components and proteins [30]. Protein carbonyls are among the most common non-enzymatic reaction products and very sensitive methods for their detection exist. The detection of protein carbonyls can thus serve as very sensitive indicator for ROS production. Here we show that protein carbonyls can be detected in cells after treatment with Ag20Pep but only marginally after treatment with Au20Pep (Figure 8A). In parallel we also followed the induction of the cytoprotective enzyme heme oxygenase 1 (HO-1), which is another established oxidative stress marker (Figure 8B) [31]. The carbonylated proteins could be enriched via immunoprecipitation (Figure 8C) and subsequent quantification demonstrated that treatment with Ag20Pep particles led to approximately 2.7-fold higher levels of protein carbonyls compared to control cells (Figure 8D).

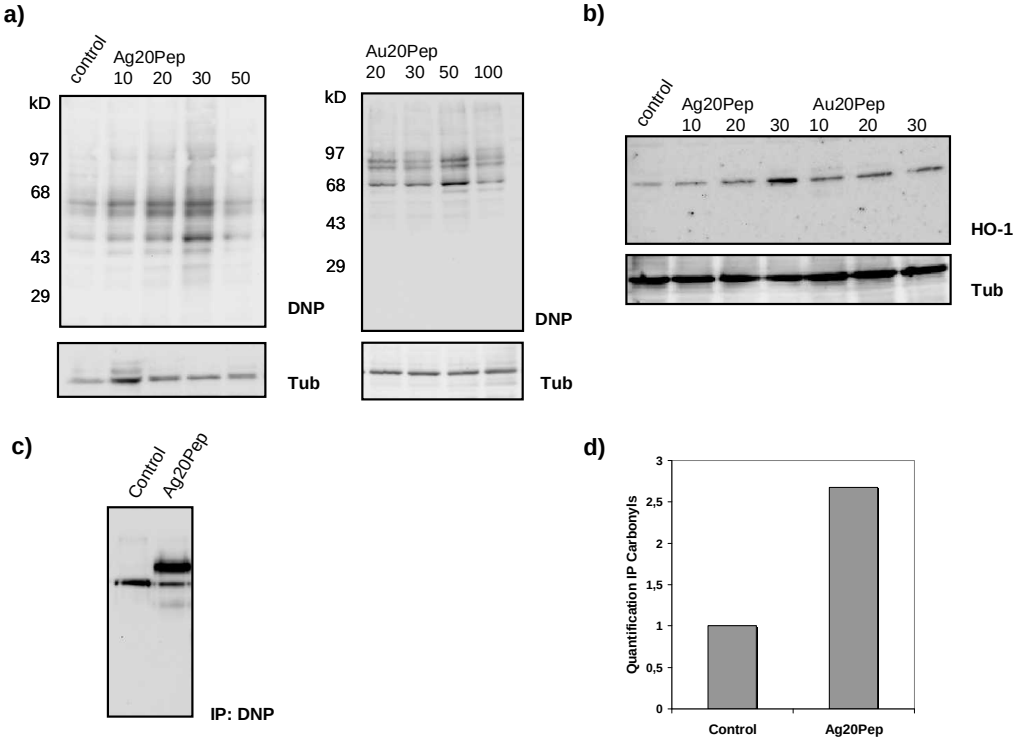

Figure 8. Oxidative stress responses in THP-1-derived macrophages after treatment with SNP. (a) Formation of protein carbonyls in cells after treatment with Ag20Pep (left panel) or Au20Pep particles (right panel). Protein carbonyls can be detected via reaction with 2,4-dinitrophenylhydrazine (DNP) to form hydrazone adducts. The doses are given in µg/ml and the treatment period was 20 h. (b) Significant induction of heme oxygenase I (HO-1) was detected in cells upon treatment with Ag20Pep particles for 20 h, but not with Au20Pep particles. All doses are given in µg/ml. (c) After formation of DNP-hydrazone adducts the carbonylated proteins were immunoprecipitated (IP) using an anbibody directed against DNP. Treatment was with 20 µg/ml Ag20Pep for 20 h. (d) Quantification of protein carbonyl levels after immunoprecipitation as shown in (c).

Protein carbonyls can also be analyzed on a 2D gel, which enables higher resolution. The differentiation between cellular reaction patterns on different types of nanoparticles can be performed with higher accuracy. Typically in a 2D gel up to 3500 different protein spots can be separated by an IPG strip approach. A typical example for a particle-induced 2D protein carbonyl pattern is shown in Figure 9.

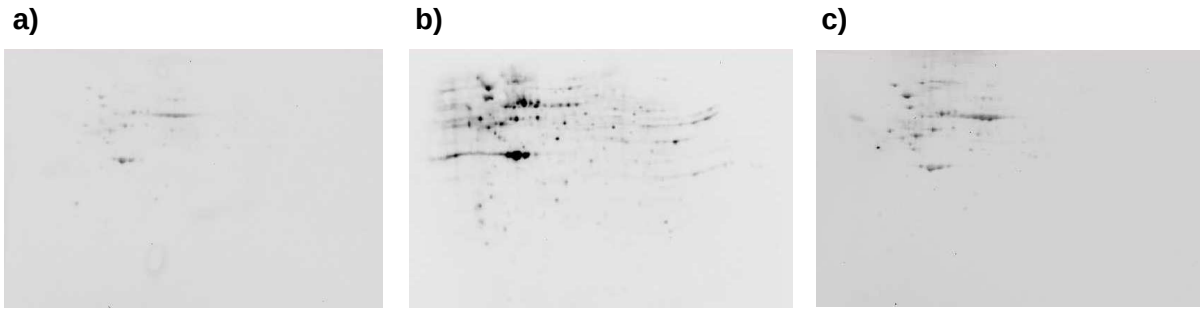

Figure 9. Detection of protein carbonyls in a 2D blot. Protein carbonyls are detectable as specific 2,4-dinitrophenylhydrazone (DNP) adducts. (a) Control cells without nanoparticle treatment. (b) 2D pattern obtained after treatment of cells with 20 µg/ml Ag20Pep particles for 20 h. (c) 2D pattern obtained after treatment of cells with 20 µg/ml Au20Pep particles for 20 h. In all gels the same amount of protein has been loaded and the resulting immunoblots were exposed for the same time period.

Finally we were interested whether or not the peptide-coated SNP do form a protein corona in cell culture media. Protein corona formation has been recently shown to occur upon contact of nanoparticles with biological fluids such as cell culture medium and there is evidence that the components of this corona affect the uptake, fate and toxicity of the particles in living systems [32,33]. In Figure 10 we show that our Ag20Pep particles indeed engage in complex protein corona formation and that some of the serum proteins become specifically enriched on the surface of the nanoparticles.

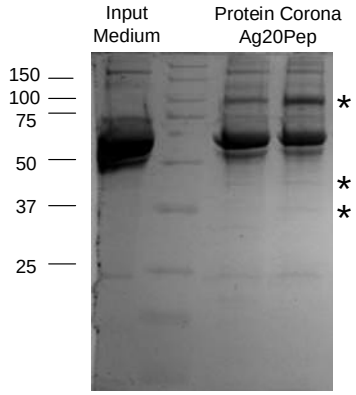

Figure 10. Protein corona formation of the Ag20Pep particles in cell culture medium. Several serum proteins are specifically enriched on the surface of the particles (marked with asterisk).

4. Discussion

Here we introduce a novel type of SNP synthesized to achieve well defined sizes and shapes and excellent colloidal properties. These SNP are nicely homogenous and display a narrow size distribution as indicated by their low polydispersity index (0.18). Classical citrate-coated particles in comparison are typically synthesized with polydispersity indices of about 0.38 and higher and thus are not as accurately defined in terms of sizes and shapes. Furthermore the new SNP form stable dispersions in aqueous environments, thereby allowing for application in toxicological studies. Indeed, the low polydispersity along with high stability against coagulation and irreversible aggregation are advantages when compared to loosely bound ligand shells. We could prove that the majority of the SNP remain individual particles inside macrophages and spread throughout cellular compartments including nuclei and nucleoli. We suggest that at least two different mechanisms of uptake exist. The larger aggregates could represent material that has been taken up via phagocytosis. By contrast, the

individual nanoparticles, which are found enriched directly underneath the cell membrane without membrane envelopes, might have been taken up by another non-phagocytic mechanism.

The peptide applied in our synthesis approach does not only play the role of a ligand, but also is crucial during first stages of nanoparticle growth, thereby allowing for both production of large scale batches and high batch-to-batch reproducibility. Especially the latter point is a very important aspect for their application in toxicity testing. Furthermore the synthesis is performed under mild and biomimetic aqueous conditions, which eliminates the possibility that organic solvents or other chemicals are subsequently transferred into cell culture systems. The surface of our nanoparticles is completely covered by the peptide, which is covalently bound. Since dissolution of the particles under these conditions seems unlikely we suggest that the majority of toxicity observed in cells is related to the nanoparticles as such and not due to the release of silver ions. This aspect will need further attention in future studies.

In addition we analyzed basic toxicity of the peptide-coated SNP. The cytotoxicity detected revealed dose- and time-dependent. The smaller SNP (*i.e.*, diameter of 20 nm) were more cytotoxic compared to the larger particles. However, if doses were calculated based on particle surfaces both types of SNP (*e.g.*, 20 nm and 40 nm diameter) appeared similar cytotoxic. We applied three independent cytotoxicity tests which delivered comparable albeit not identical results. In recent days, nanosilver becomes available in a variety of different shapes, coatings and sizes. Since we are particularly interested to compare the toxicity of the peptide-coated nanoparticles with other types of SNP that can be obtained through rather conventional syntheses, we started to look into the cytotoxicity of peptide-coated SNP *versus* citrate-coated SNP of the same size (20 nm). Preliminary results show that citrate-coated SNP exert only little cytotoxicity in THP-1 cell cultures up to concentrations of 200 µg/ml (data not shown). It will be interesting to include other types of SNP including pristine nanosilver to better characterize the influence of the different coating on the cellular responses observed.

We also demonstrate that exposure to 20 nm SNP triggers significant oxidative stress insides macrophages, thereby clearly contrasting the absence of such effects after treatment with nanogold. At all endpoints addressed the peptide-coated nanogold only induced very faint responses, if any, and thus may be considered biologically inert. Oxidative stress was demonstrated by analyzing two different responses. Besides particle-mediated induction of HO-1, we could indirectly show the formation of ROS via detection of protein carbonyls. The protein carbonyl species generated within cells could be further separated by means of 2D gel chromatography. With this approach we show that nanosilver treatment leads to significant increases in the intracellular levels of protein carbonyls when compared to nanogold or cells without treatment. The patterns of protein carbonyls obtained with nanogold-treated cells were similar to untreated cells.

In nanotoxicology there is some debate on the issue of whether or not it may be justifiable to compare results obtained *in vitro* with those expected to occur *in vivo*. This is due to the fact that in *in vitro* studies one bolus dose is delivered, which usually is rather high. By contrast, during *in vivo* studies typically lower doses are delivered over a longer period of time. In our study we observed strongest effects in terms of oxidative stress in a concentration range of 20-30 µg/ml SNP. Taking the density of silver (0.01049 ng/cm^3) under the assumption that particles are ideally spheric, this concentration range equals a particle number range of 5.7 – 8.5 x 10^{10}/ml. A regular cell density of 1.5 x 10^5 cells/ml then results in the highest observed effect at the external dose of 0.38 to 0.57 x 10^6 particles per cell. To become clear about the concentration range, we compare this to a regular 28-days rat inhalation study published in 2007 [11]. In this study rats were exposed for 6 h per day and 5 days a week to SNP with sizes ranging between 1.9 and 65 nm diameter. The doses applied were low (1.74 x 10^4 particles/cm^3), medium (1.27 x 10^5 particles/cm^3) or high (1.32 x 10^6 particles/cm^3), with the highest dose equaling 61 µg/m^3. Considering the average weight and the breath volume (0.29 m^3/kg) of the animals results in an exposure level of approximately 1.4 x 10^9 (low dose) to 1.1 x 10^{11} particles (high dose) per day. For the complete 4-week period this would equal 2.83 x 10^{10} (low dose) to 2.16 x 10^{12} particles (high dose). Taking these numbers into account we

conclude that the concentrations applied in our study *in vitro* to obtain maximal effects (5.7 – 8.5 x 10^{10} particles/ml) were in a comparable range to what will get inhaled within one day (6 hours) by the lungs of animals exposed to a dose of 1.32 x 10^6 particles/cm^3. Certainly, for the *in vivo* situation this is only a rough estimation. Typically in the bronchoalveolar lavage of one rat a total of 5 x 10^6 cells can be found [34]. In our study we used 1.5 x 10^5 cells for each treatment. In comparison to other *in vitro* studies that regularly use treatment doses of up to 100-200 µg/ml, we already observed strongest effects in the comparably low range of 20-30 µg/ml (10-15 µg/cm^2) that was proven well below the threshold level of cytotoxicity.

Acknowledgments
The authors acknowledge excellent technical assistance of Annika-Mareike Gramatke, Antje Bergert, Doreen Wittke and Monika Sachtleben. A. Mantion thanks BAM for an Adolf-Martens Fellowship. The authors are grateful to the following institutions for financial support: Swiss National Science Foundation, Federal Institute for Risk Assessment (BfR), Federal Institute for Material Research and Testing (BAM), The Free University of Berlin, University of Potsdam, Fonds der Chemischen Industrie and MPI of Colloids and Interfaces (Colloid Chemistry Department).

References
[1] Edward-Jones V 2009 The benefits of silver in hygiene, personal care and healthcare *Lett. Appl. Microbiol.* **49** 147-52
[2] Chen X and Schluesener H J 2008 Nanosilver: a nanoproduct in medical application *Toxicol. Lett.* **176** 1-12
[3] Jain J, Arora S, Rajwade J M , Omray P, Khandelwal S and Paknikar K M 2009 Silver nanoparticles in therapeutics: development of an antimicrobial gel formulation for topical use *Mol. Pharm.* **6** 1388-1401
[4] Eby D M, Luckarift H R and Johnson G R 2009 Hybrid antimicrobial enzyme and silver nanoparticle coatings for medical instruments *ACS Appl. Mater. Interfaces* **1** 1553-60
[5] Lee H Y, Park H K, Lee Y M, Kim K and Park S B 2007 A practical procedure for producing silver nanocoated fabric and its antibacterial evaluation for biomedical applications *Chem. Commun.* **28** 2959-61
[6] Vigneshwaran N, Kathe A A, Varadaraian P V, Nachane R P and Balsubramanva, R H J 2007 Functional finishing of cotton fabrics using silver nanoparticles *Nanosci. Nanotechnol.* **7** 1893-97
[7] Kokura S, Handa O, Takagi T, Ishikawa T, Naito Y and Yoshikawa T 2010 Silver nanoparticles as a safe preservative for use in cosmetics. *Nanomedicine* **6** 570-74
[8] Hoet P, Brueske-Hohlfeld I and Salata O V 2004 Nanoparticles— known and unknown health risks *J. Nanobiotechnol.* **2** 12-27
[9] Seaton A, Tran L, Aitken R and Donaldson K 2010 Nanoparticles, human health hazard and regulation. *J. R. Soc. Interface* **7** Suppl. 1 S119-29
[10] Xia T, Li N and Nel A E 2009 Potential health impact of nanoparticles *Annu. Rev. Public Health* **30** 137-50
[11] Ji J H, Jung J H, Kim S S, Yoon J U, Park J D, Choi B S, Chung Y H, Kwon I H, Jeong J, Han B S, Shin J H, Sung J H, Song K S and Yu I J 2007 Twenty-eight-day inhalation toxicity study of silver nanoparticles in Sprague-Dawley rats *Inhal. Toxicol.* **19** 857-71
[12] Tang J, Xiong L, Wang S, Wang J, Liu L, Li J, Yuan F and Xi T 2009 Distribution, translocation and accumulation of silver nanoparticles in rats *J. Nanosci Nanotechnol.* **9** 4924-32
[13] Larese F F, D'Agostin F, Grosera M, Adami G, Renzi N, Bovenzi M and Maina G 2009 Human skin penetration of silver nanoparticles through intact and damaged skin *Toxicology* **255** 33-7
[14] Greulich C, Kittler S, Epple M, Muhr G and Koller M 2009 Studies on the biocompatibility and

the interaction of silver nanoparticles with human mesenchymal stem cells (hMSCs) *Langenbecks Arch. Surg.* **394** 495-502
[15] Foldbjerg R, Olesen P, Hougaard M, Dang D A, Hoffmann H J and Autrup H 2009 PVP-coated silver nanoparticles and silver ions induce reactive oxygen species, apoptosis and necrosis in THP-1 monocytes *Toxicol. Lett.* **190** 156-62
[16] AshaRani P V, Low Kah Mun G, Hande M P and Valiyaveettil S 2009 Cytotoxicity and genotoxicity of silver nanoparticles in human cells *ACS Nano* **3** 279-90
[17] Carlson C, Hussain S M, Schrand A M, Braydich-Stolle L K, Hess K L, Jones R L and Schlager JJ 2008 Unique cellular interaction of silver nanoparticles: size-dependent generation of reactive oxygen species *J. Phys. Chem. B.* **112** 13608-19
[18] Li N, Xia T and Nel A E 2008 The role of oxidative stress in ambient particulate matter-induced lung diseases and its implications in the toxicity of engineered nanoparticles *Free Radic. Biol. Med.* **44** 1689-1699
[19] Arora S, Jain J, Rajwade J M and Paknikar K M 2008 Cellular responses induced by silver nanoparticles: *in vitro* studies *Toxicol. Lett.* **179** 93-100
[20] Ivask A, Bondarenko O, Jepihhina N and Kahru A 2010 Profiling of the reactive oxygen species-related ecotoxicity of CuO, ZnO, TiO2, silver and fullerene nanoparticles using a set of recombinant luminescent *Escherichia coli* strains: differentiating the impact of particles and solubilized metals *Anal. Bioanal. Chem.* **398** 701-16
[21] Lubick N 2008 Nanosilver toxicity: ions, nanoparticles— or both? *Environ. Sci. Technol.* **42** 8617
[22] Lankveld D P, Oomen A G, Krystek P, Neigh A, Troost-de Jong A, Noorlander C W, Van Eijkeren J C, Geertsma RE and De Jong W H 2010 The kinetics of the tissue distribution of silver nanoparticles of different sizes *Biomaterials* **31** 8350-61
[23] Sur I, Cam D, Kahraman M and Baysal A 2010 Interaction of multi-functional silver nanoparticles with living cells *Nanotechnology* **21** 175104
[24] Pal S, Tak Y K and Song J M 2007 Does the antibacterial activity of silver nanoparticles depend on the shape of the nanoparticle? A study of the gram-negative bacterium *Escherichia coli*. *Appl. Environ. Microbiol.* **73** 1712-20
[25] Mantion, A, Massuger L, Rabu P, Palivan C, McCusker L B and Taubert A 2008 Metal-peptide frameworks (MPFs) : « Bioinspired » metal organic frameworks *J. Am. Chem. Soc.* **130** 2517-26
[26] Dickerson M B, Sandhage K H and Naik R R 2008 Protein- and peptide-directed syntheses of inorganic materials. *Chem. Rev.* **108** 4935-78
[27] Mantion A, Guex A G, Foelske A, Mirolo L, Fromm K M, Painsi M and Taubert A 2008 Silver nanoparticle engineering via oligovaline organogels *Soft Matter* **4** 606-617
[28] Graf P, Mantion A, Foelske A, Shkilnyy A, Masic A, Thuenemann A F and Taubert A 2009 Peptide-coated silver nanoparticles: synthesis, surface chemistry, and pH-triggered, reversible assembly into particles assemblies *Chem. Eur. J.* **15** 5831-44
[29] Nehring R, Palivan C G, Moreno-Flores S, Mantion A, Tanner P, Toca-Herrera J L, Thuenemann A, and Meier W 2010 Protein decorated membranes by specific molecular interactions *Soft Matter* **6** 2815-24
[30] Dalle-Donne I, Carini M, Vistoli G, Ragazzoni L, Colombo G, Rossi R, Milzani A and Aldini G. 2009 Protein carbonylation: 2,4-dinitrophenylhydrazine reacts with both aldehydes/ketones and sulfenic acids *Free Radic. Biol. Med.* **46** 1411-19
[31] Xia T, Kovochnich M, Brant J, Hotze M, Sempf J, Oberley T, Sioutas C, Yeh J, Wiesner M R and Nel A E 2006 Comparison of the abilities of ambient and manufactured nanoparticles to induce cellular toxicity according to an oxidative stress paradigm *Nano Lett.* **6** 1794-1807
[32] Lundqvist M, Stigler J, Elia G, Lynch I, Cedervall T, Dawson K A 2008 Nanoparticle size and surface properties determine the protein corona with possible implications for biological impacts *Proc. Natl. Acad. Sci. USA* **105** 14265-14270

[33] Lynch I, Dawson K A 2008 Protein-nanoparticle interactions *Nano Today* **3** 40-48
[34] Pauluhn J 2007 Pulmonary toxicity and fate of agglomerated 10 and 40 nm aluminium oxyhydroxides following 4-week inhalation exposure of rats: toxic effects are determined by agglomerated, not primary particle size *Toxicol. Sci.* **109** 152-167
[35] Auwerx J 1991 The human leukaemia cell line, THP-1: a multifaceted model for the study of monocyte-macrophage differentiation *Experientia* **47** 22-31
[36] Park E K, Jung H S, Yang H I, Yoo M C, Kim C and Kim K S 2007 Optimized THP-1 differentiation is required for the detection of responses to weak stimuli *Inflamm. Res.* **56** 45-50
[37] Richardson K C, Jarett L and Finke E H 1960 Embedding in epoxy resins for ultrathin sectioning in electron microscopy *Stain Technol.* **35** 313-23